ACS APPLIED MATERIALS & INTERFACES

Research Article

Cite This: ACS Appl. Mater. Interfaces 2019, 11, 11706−11714

www.acsami.org

Fabrication of Hydrazone-Linked Covalent Organic Frameworks Using Alkyl Amine as Building Block for High Adsorption Capacity of Metal Ions

Ya Li,[†,‡] Chang Wang,[†] Shujuan Ma,[†,‡] Haiyang Zhang,[†,‡] Junjie Ou,*[,†] Yinmao Wei,*[,‡] and Mingliang Ye[†]

[†]CAS Key Laboratory of Separation Science for Analytical Chemistry, Dalian Institute of Chemical Physics, Chinese Academy of Sciences, Dalian 116023, China

[‡]Key Laboratory of Synthetic and Natural Function Molecule Chemistry of Ministry of Education, College of Chemistry and Materials Science, Northwest University, Xi'an 710069, China

Supporting Information

ABSTRACT: There are several researches on the preparation and application of hydrazone-linked covalent organic frameworks (COFs), and all of them generally necessitate rigid aromatic amines. Herein, we report a strategy for design and synthesis of COF with flexible alkyl amine as a building block and intramolecular hydrogen bonding as a knot in the network. The proof-of-concept design was demonstrated by exploring 1,3,5-triformylphloroglucinol and oxalyldihydrazide (ODH) as precursors to synthesize a novel COF material (TpODH), in which different organic building units are combined through hydrazone bonds to form two-dimensional porous frameworks. It should be pointed that irreversible enol-to-keto tautomerism and intramolecular N−H···O═C hydrogen bonding of TpODH would enhance the crystallinity and chemical stability, leading to large specific surface area of 835 m^2 g^{-1}. However, another COF synthesized with 1,3,5-triformylbenzene and ODH exhibited less crystallinity and low special surface area (94 m^2 g^{-1}). Representatively, the resulting TpODH afforded Cu(II) and Hg(II) capacities of 324 and 1692 mg g^{-1}, respectively, which exceeded that of most COFs previously reported. Moreover, the Fourier-transform infrared and X-ray photoelectron spectroscopy spectra analyses were taken to demonstrate the adsorption mechanism. These results suggested that the materials could be applied to the removal of metallic ions in the future.

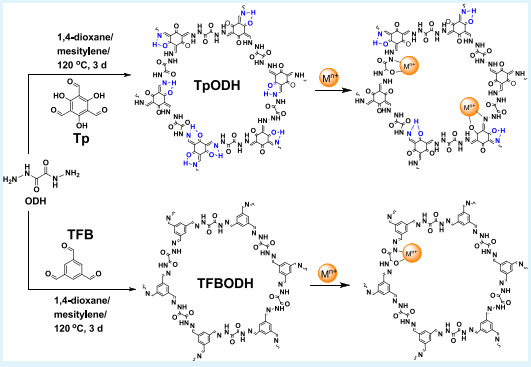

KEYWORDS: *flexible alkyl amine, covalent organic frameworks, intramolecular hydrogen bonding, metal ions adsorption, high capacity, selectivity adsorption*

INTRODUCTION

Due to the particular characteristics and enormous potentials, covalent organic frameworks (COFs)[1] have attracted considerable scientific attention. COFs are porous extended crystalline materials that absolutely consist of covalent bonds between light elements, such as C, H, N, O, and B, which crystallize into regular frameworks that are beneficial for detection by original molecular building blocks. Since first discovered in 2005,[2] many COFs have been synthesized by different condensation reactions using well-known covalent bonds, including boronate,[3] boroxine,[4] imine,[5] and hydrazone[6] linkages. These COFs show tunable functionalities, regular pore structures, and high surface areas. Therefore, it is significant prospect of COFs to address current challenges pertinent to energy and environmental sustainability, including gas adsorption, catalysis, proton conduction, and so on.[6−10]

The functional groups and tunable nature of COFs may also be beneficial in mitigating environmental problems caused by toxic heavy metals. First, functional groups on the COF not only affect the adsorption selectivity but also dominate the adsorption mechanism. Adsorbents with carboxyl, sulfonic, and phosphonic groups remove adsorbates through ion exchange,[11,12] whereas others containing nitrogen such as amine and hydrazine adsorb metal ions through both electrostatic and coordination interactions.[13,14] Especially, amine groups are among the most effective groups for the removal of heavy metal ions from aqueous solutions.[15,16] Second, both "bottom-up"[17] and "post-synthesis"[18] strategies could be applied to attach specific moieties into the COF framework. Thus, the selective sensing toward diverse applications may be easily achieved. We speculate that such materials, in particular, two-dimensional (2D) COFs, have the right combination of properties that give them potential as excellent sorbents for environmental remediation. The ordered

Received: October 24, 2018
Accepted: March 8, 2019
Published: March 8, 2019

DOI: 10.1021/acsami.8b18502
ACS Appl. Mater. Interfaces 2019, 11, 11706−11714

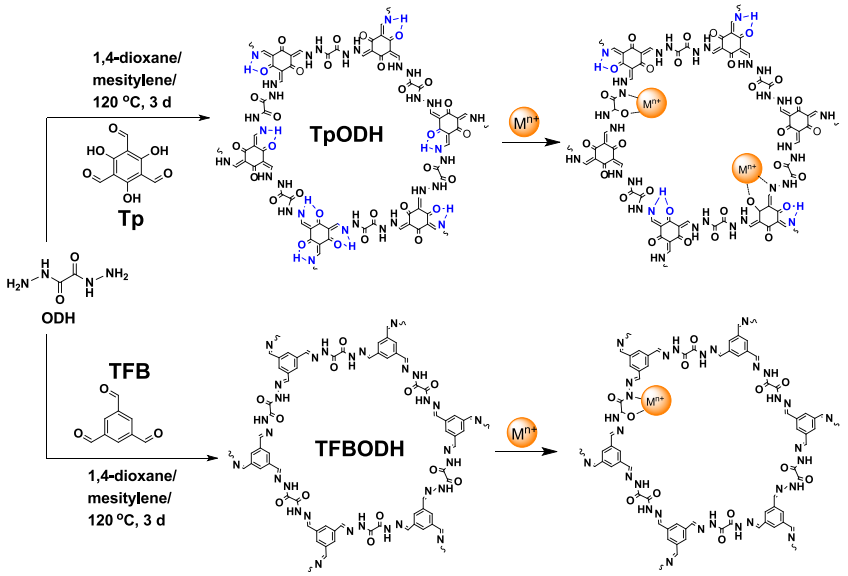

Figure 1. Schematic of the construction of hydrazone-linked COFs and their metal chelates.

π-columnar structures of most 2D COFs enabled the functional groups to be fully accessible and in close proximity with each other to facilitate their cooperation.

Particularly, the number of reported imine-linked COFs has increased dramatically because of easily thinkable as-synthesized aromatic monomers and comparatively high stability of the imine. However, the limited amount of nitrogen and oxygen groups on the surface inevitably diminishes the population density of chelating sites, resulting in low saturation capacity and affinity. Given the aforementioned limitation, there is a need for the development of new COFs with unique characteristic. It should be pointed that there are some researches on hydrazone linkages COFs,[19−23] but most of them exhibited relatively low surface area (less than 600 m^2 g^{-1}) and provided access to only a limited number of structural motifs.

Here, we first selected oxalyldihydrazide (ODH) and 1,3,5-triformylphloroglucinol (Tp) as precursors to generate crystalline porous COFs. The obtained 2D COF (TpODH) showed more excellent property including good crystallinity and large specific surface area. Porosity in the COF is beneficial for the interaction between adsorbate and binding sites, more importantly, the high density of N and O elements on the TpODH skeleton inevitably increases the density of coordination sites, thus resulting in high metal-loading capability and affinity. Another nonhydroxyl COF analogue (TFBODH) was also synthesized by using 1,3,5-triformylbenzene (TFB) and ODH.

RESULTS AND DISCUSSION

Synthesis, Characterization, and Stability Analysis. There were a few hydrazone-linked COFs typically synthesized with aromatic amines, such as benzene-1,3,5-tricarbohydrazide,[24] 2,5-diethoxyterephthalohydrazide,[25−27] and pyromellitic-*N*,*N*′-bisaminoimide.[28] Nowadays, it is still a great challenge to fabricate COFs frameworks using flexible alkyl amines. Herein, introducing intramolecular C═O···H−N hydrogen bonding between C═O of Tp (enol-to-keto) and H−N of ODH will decrease the possibility in different linker lengths of ODH and form uniform directionalities, which are an advantage in enhancing crystallinity, porosity, and chemical stability of COF.[29] To validate our approach, a new 2D COF was synthesized by combining ODH with Tp in a 3:2 molar ratio. For comparison, another monomer TFB was also chosen for the preparation of nonhydroxyl COF analogue. Previous studies[30,31] have shown that Cu(II) and Hg(II) tend to form stable chelates with N- and O-containing functional groups, thus ODH was selected as one of the linker. As shown in Figure 1, two hydrazone-linked COFs (TpODH and TFBODH) were prepared under solvothermal conditions by condensation reaction of ODH and Tp and TFB, respectively, with acetic acid as catalyst. Subsequently, metal ions (M^{n+}) could form stable chelates through coordination interaction with TpODH and TFBODH. The reaction conditions played vitally important roles on crystallinity and specific surface area of the resulting frameworks. To gain ideal COF crystals, a variety of reaction solvents, including dioxane, mesitylene, *o*-dichlorobenzene (DCB), dimethylacetamide (DMAc), and *o*-DCB/DMAc were investigated, as shown in Figure S2, Supporting Information (SI). In addition, other factors including reaction time and temperature and the concentration of monomer and catalyst were also optimized. After carefully optimizing the preparation conditions, a binary system of mesitylene/dioxane (1:1 v/v) was explored to synthesize TpODH and TFBODH at 120 °C for 3 days in the presence of HAc (6 M).

The atomic-level construction of TpODH and TFBODH was assessed by high-resolution Fourier-transform infrared (FT-IR) and sNMR spectroscopy. FT-IR spectrum of TpODH (Figure 2a) presented obvious peaks at 1237 cm^{-1} of −C−N− stretch and 1540 cm^{-1} of −C═C− stretch, which belong to the characteristic signal of β-ketoenamine linkages.[32] For Tp, two characteristic peaks at 1640 and 2891 cm^{-1} belong to aldehyde group (Figure 2b). Compared to Figure S3b,c, a peak at 1628 cm^{-1} could be observed in Figure S3a, which was assigned to the −C═N− stretch in TFBODH, indicating the formation of imine bonds. Furthermore, there were distinct differences in the wave numbers of carbonyl and N−H stretching between TpODH and TFBODH, which changed from ≈1680 and ≈3426 cm^{-1} (TFBODH) to ≈1640 and ≈3370 cm^{-1} (TpODH), respectively. The formation of

DOI: 10.1021/acsami.8b18502
ACS Appl. Mater. Interfaces 2019, 11, 11706−11714

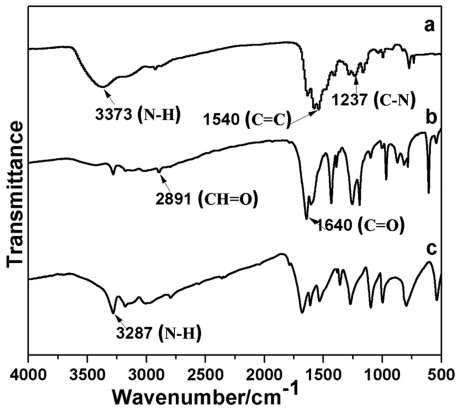

Figure 2. High-resolution FT-IR spectra of (a) TpODH, monomers, (b) Tp, and (c) ODH.

intramolecular C═O···H−N hydrogen bonding in TpODH was convincingly demonstrated. More detailed information was given by ^{13}C NMR analysis. As shown in Figure 3a, the

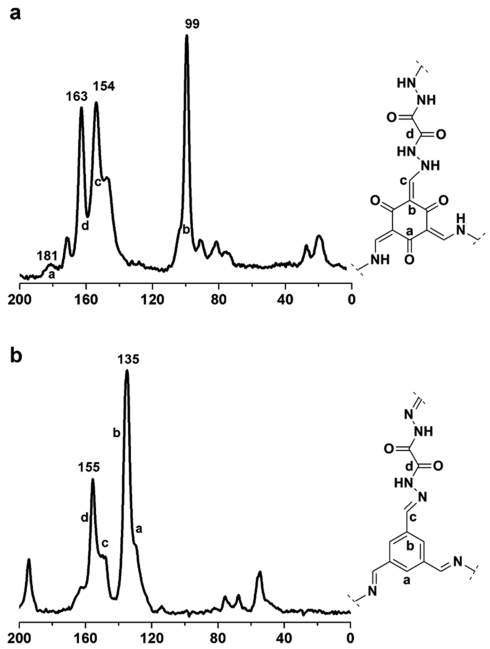

Figure 3. ^{13}C NMR spectra of (a) TpODH and (b) TFBODH.

resonance at 99 ppm was assigned to the exocyclic carbons (C═C) in TpODH, and the resonance signal at 181 ppm assigned to the carbonyl carbons (C═O) of quaternary carbons (ring). Correspondingly, the signal at 155 ppm in Figure 3b indicated the formation of −C═N− in TFBODH, which overlapped absolutely with the peak of C═O carbons, and the signal at 135 ppm could correspond to the carbon atoms of benzene ring on the framework. As mentioned above, it further corroborated the molecular backbones of TpODH and TFBODH.

As shown in Figure 4, the morphology of two COFs was characterized by helium ion microscopy (HIM) and TEM.

It could be observed from Figure 4a that TpODH crystallized with a flowerlike morphology, which was similar to two reported COFs prepared with Tp and aromatic diamines, *p*-phenylenediamine (PDA) and 2,5-dimethyl-*p*-phenylenediamine.[33] In this system, each individual flower unit could be deemed to be a collection of plentiful petals about 2 μm long, 150−300 nm wide, and 20−40 nm thick, forming a platelike structure. In the case of TFBODH (Figure 4c), the petals were much broader and longer, were 500−1000 nm wide, were 80−100 nm thick, had regular spike shape, and grew out long-order structure from a core. Furthermore, the TEM images were also used to certify these flowerlike morphologies (Figure 4b,d), which manifested that these individual petals had a sheetlike characteristic because of the $\pi-\pi$ stacking in the skeleton of the COF layers.

The powder X-ray diffraction (PXRD) measurements of the synthesized bulk material confirmed the regular crystalline structure of TpODH and TFBODH. According to the experimental PXRD patterns in Figure 5, the peaks of TpODH and TFBODH were remarkably different from those of the three precursors.

The PXRD patterns of TpODH exhibited a strong peak at 4.5° (±0.2, 2θ), with *d* spacing of 19.4 Å, which corresponded to the reflection from the 100 plane (Figure 5). Meanwhile, a relatively broad peak emerged at higher 2θ value (~27.6° ± 0.2), with *d* spacing of 3.2 Å because of the reflection from the 100 plane, indicating the $\pi-\pi$ stacking between successive layers of COF. As shown in Figure 5, a weak peak at 4.8° (±0.2, 2θ) with *d* spacing of 18.3 Å arose also corresponding to the 001 plane reflection in TFBODH, whose shift to a higher 2θ value was attributed to smaller pore aperture. By comparison, the peak intensity in TFBODH was slightly lower than that in TpODH, indicating poor crystallinity of TFBODH. Additionally, the unit cells of TpODH and TFBODH were also calculated at the B3LYP/6-311++(d, p) level with Gaussian 09 package,[34] and their pore size was 19.9 and 18.3 Å (Figure S4a,b), respectively, which perfectly matched with the experimental results. Compared to previous two kinds of COFs, Tp−PDA COF[35] prepared with Tp and PDA and COF-LZU1[12] synthesized with TFB and PDA, more insight into the structure of COF could be gained. As shown in Figure S4c,d, the molecular size of ODH is close to that of PDA, which was also calculated with density functional theory and the Multiwfn[36] program package. According to the (100) diffraction of Tp−PDA, 2θ value was 4.68°, indicating the most intense and lowest 2θ value peak with *d* spacing of 18.9 Å. As for COF-LZU1, 2θ value was 4.72°, with *d* spacing of 18.7 Å. As a result, *d* spacing of TpODH and TFBODH was close to that of Tp−PDA and COF-LZU1, respectively. In addition, the calculated gas-phase rotational barrier of ODH C−N bond was 4.05 kcal mol^{-1} at the B3LYP/6-311++(d, p) level (Figure S4e), which was especially lower than that of amides.[37] It is inevitable that the synthesized COF crystal adopted various linked lengths and directionalities, as ODH units might have different conformations under the solvothermal conditions. For crystalline growth of COFs, the process of dynamic error correction is essential; nevertheless, this linkage flexibility would increase the potential for crystallographic defects.

Nitrogen sorption isotherm was taken on the activated samples at 77 K to estimate the permanent porosity of as-synthesized COFs (Figures 6a and S5a). The resulting BET surface areas of two materials were 835 (TpODH, Figure S5c) and 94 m^2 g^{-1} (TFBODH, Figure S5d), whereas the Langmuir surface areas for TpODH (Figure S5e) and TFBODH (Figure S5f) were 1183 and 164 m^2 g^{-1}, respectively. For TFBODH, these lower values were due to the linkage flexibility and pore deformation as a result of framework flexibility.[38] At P/P_0 =

DOI: 10.1021/acsami.8b18502
ACS Appl. Mater. Interfaces 2019, 11, 11706−11714

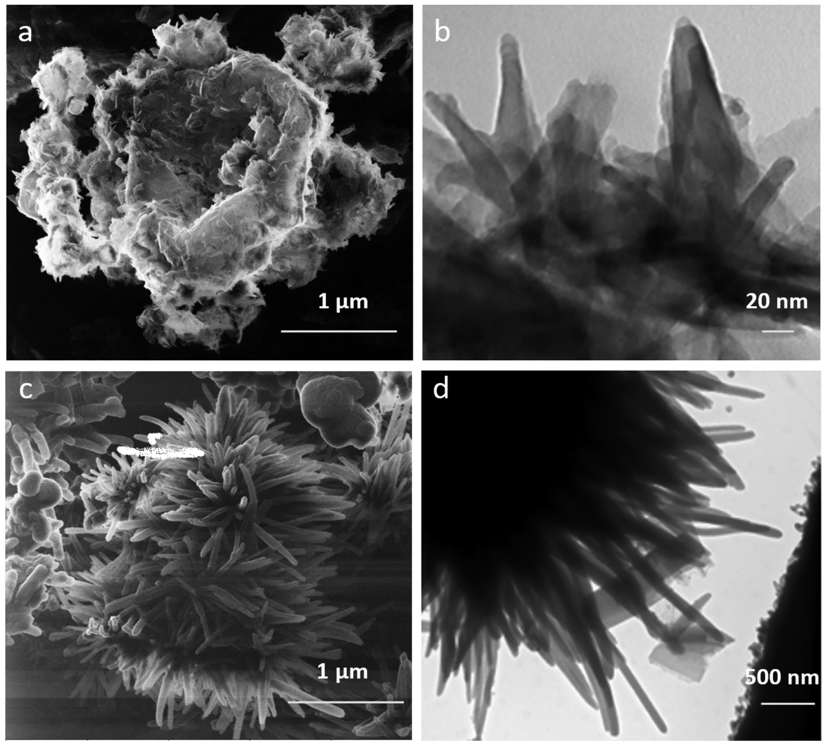

Figure 4. (a, c) HIM and (b, d) TEM images of (a, b) TpODH and (c, d) TFBODH showing a nanoflower morphology.

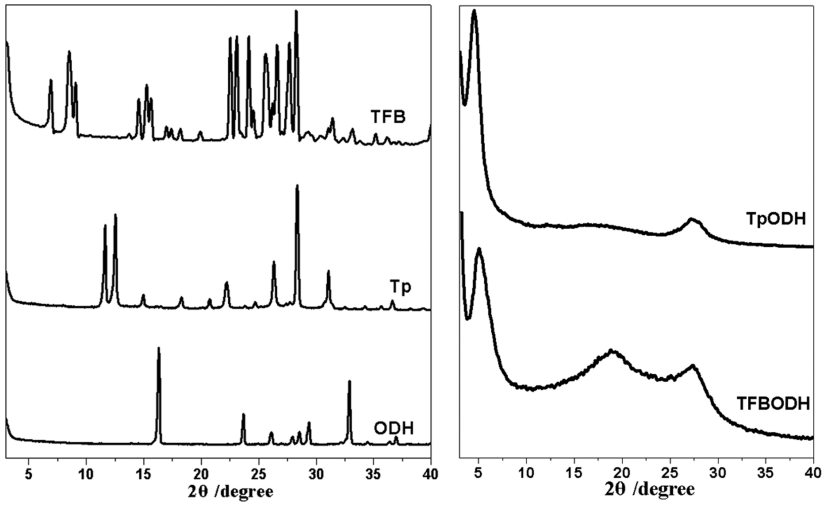

Figure 5. PXRD patterns of monomers TFB, Tp, ODH, and two COFs TpODH and TFBODH.

0.99, the total pore volumes of the two materials were evaluated to be 0.89 and 0.15 $cm^3\ g^{-1}$, respectively. A micropore size distribution (0.5−1.2 nm) for TpODH (Figure 6b) was obtained using nonlocal density functional theory (NLDFT) model. The same model was fitted to isotherms of TFBODH (Figure S5b) to estimate its pore size distribution. The irregular pore size distribution is very likely associated with textural porosity arising from the packing of the COF domains; on the other hand, these 2D materials may lack sufficient long-range ordering structure, which could be observed from the XRD patterns.[39]

To realize the widespread application, it is essential to evaluate the stability of COFs. PXRD patterns were used to certify the chemical stability of TpODH and TFBODH after two days treatment in boiling water, HCl (9 M) and NaOH (9 M) aqueous solutions at room temperature. As demonstrated in Figure 6c, TpODH was stable in boiling water and aqueous HCl as evident from the PXRD patterns without distinct difference in the peak position and intensity. Furthermore, it was extremely persuasive that crystallinity was largely stable under different harsh conditions, even though immersion in 9 M NaOH led to only a slight decrease in the peak intensities. This feature is superior to other popular adsorbents, such as silica- or metal−organic frameworks-based ones, which easily suffer from the distortion of skeleton under harsh conditions. However, the mass of TFBODH was greatly reduced, and the remaining material's crystallinity was poor and nearly rendered amorphous (Figure S6, SI). The thermogravimetric analysis of both TpODH and TFBODH in N_2 atmosphere exhibited identical thermal stability up to ∼300 °C, manifesting high

DOI: 10.1021/acsami.8b18502
ACS Appl. Mater. Interfaces 2019, 11, 11706−11714

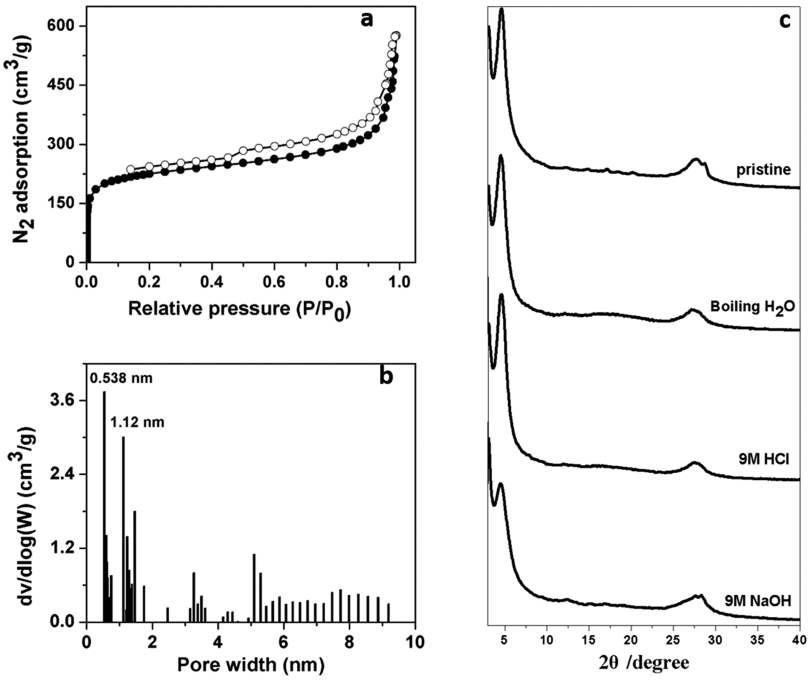

Figure 6. (a) N_2 adsorption isotherm (77 K), (b) pore size distribution profiles calculated according to NLDFT model, and (c) PXRD patterns after treatment in different systems of TpODH.

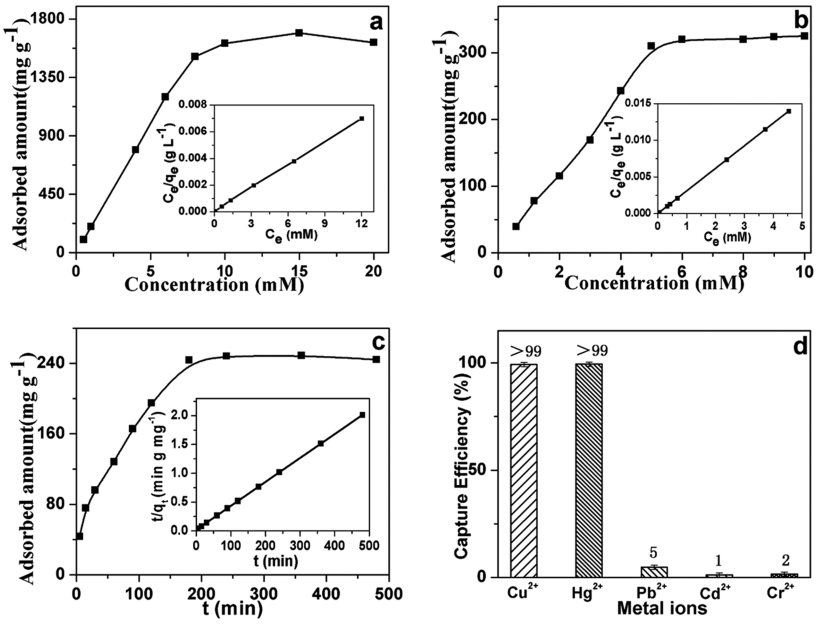

Figure 7. (a) Hg(II) adsorption isotherm of TpODH at room temperature. Inset shows the linear regression with the Langmuir adsorption model by fitting the isotherm. (b) Cu(II) adsorption isotherm of TpODH at room temperature. Inset shows linear regression with the Langmuir model. (c) Adsorption kinetic of Cu(II). Inset presents the pseudo-second-order kinetic plot for the adsorption process of TpODH to Cu(II). (d) Capture efficiency in removing different metal ions.

thermal stability of all as-synthesized COFs. As we all know, the melting point of the crystallizable compound will be influenced by the presence of impurity, including solvent or second polymer. For some crystallizable polymer with weak interactions, the melting point compromise is not obvious but is of significance in hydrogen-bonded system. Compared to TFBODH (226 °C), the melting point of TpODH (219 °C) showed a slight decrease due to H-bonding (Figure S7, SI).

Adsorption of Metal Ions. Two-dimensional materials with abundance of nitrogen and $\pi-\pi$-conjugated system may provide more possibility for their interaction with metal ions. To assess the adsorption ability of TpODH, adsorption isotherms for copper, mercury, lead, chromium, and cadmium were plotted after measuring five metal ions' aqueous solutions with different concentrations. When researching the adsorption process, adsorption isotherm should be considered first, which could exactly describe how they interact with each other between analytes and adsorbent. As shown in Figure 7a, it should be highlighted that TpODH has an adsorption capacity of Hg(II) of about 1692 mg g^{-1}. Considering the extraordinary

DOI: 10.1021/acsami.8b18502
ACS Appl. Mater. Interfaces 2019, 11, 11706−11714

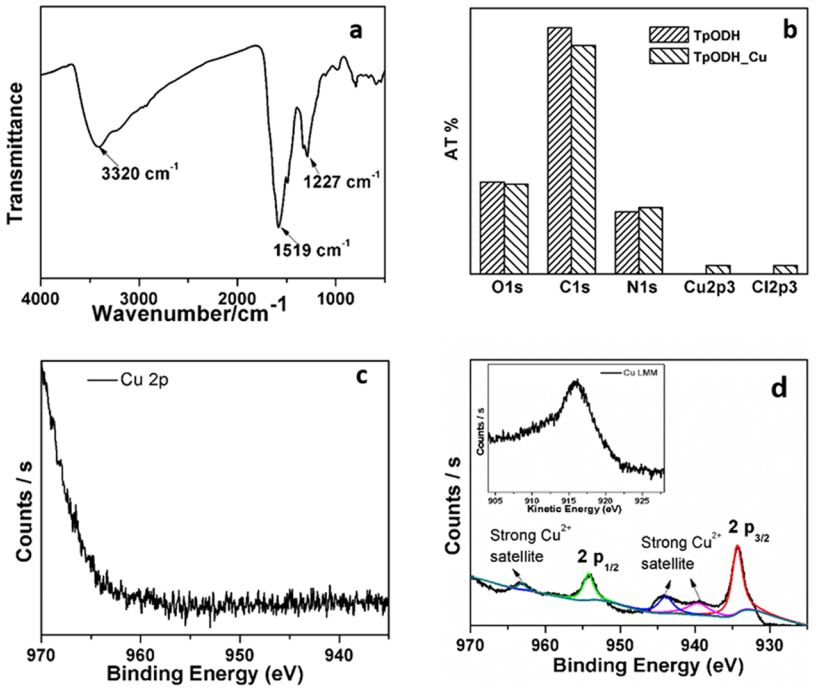

Figure 8. (a) FT-IR spectra of TpODH_Cu, (b) elemental composition of TpODH and TpODH_Cu, and XPS spectra of (c) TpODH and (d) TpODH_Cu. Inset shows the Cu LMM spectra of ODH_Cu XPS bands of Cu(II).

binding ability of sulfur with mercury, there are two kinds of COFs[40,41] that were decorated with sulfur and used for mercury removal. The adsorption capacity of the above reported two COFs was 1350 and 734 mg g^{-1}, respectively. Considering the strong electrophilicity of Hg(II), the binding site on the adsorbent needs to have abundant electron (N, O, S, etc.) to make a strong interaction.[42] TpODH with high density of nitrogen and oxygen would contribute to the capture of mercury. Then, the Langmuir adsorption model was selected to investigate the adsorption mechanism of mercury on TpODH. It could be clearly observed that the achieved equilibrium adsorption isotherm was well matched with the Langmuir model and resulted in a high correlation coefficient (R_L > 0.998). This result demonstrated that the adsorption process would be monolayer.

As shown in Figure 7b, the saturated adsorbed amount of TpODH to Cu(II) was calculated to be 324 mg g^{-1}, whereas another COF TFBODH (Figure S8a) was only 23 mg g^{-1}. Particularly, this adsorbed amount of TpODH to Cu(II) was remarkably higher than those of the published materials, including commercial resins (166 mg g^{-1})[43] and multiwalled carbon nanotubes (24.5 mg g^{-1}).[44] The outstanding capacity should be ascribed to the plentiful nitrogen and oxygen covered on the skeleton of TpODH, facilitating to trap Cu(II). The adsorption isotherm of Cu(II) was found to follow a Langmuir model with the correlation coefficient as high as 0.999 (Figure 7b). As presented in Figure 7c, pseudo-second-order kinetic model was used to fit the kinetic data of copper and interpret the mechanism of adsorption process. It can be proven by fitting the experimental data with the pseudo-second-order kinetic model using eq S2 (SI). High correlation coefficient (0.999) demonstrated that pseudo-second-order kinetic model was fitted for the adsorption of Cu(II) onto the surface of TpODH. As mentioned above, the adsorption process was chemical adsorption between COF and metal ion. Distribution coefficient (K_d) was used to value the affinity of adsorbent to adsorbate, and K_d value of 1.0×10^4 mL g^{-1} was generally regarded as excellent affinity of material for copper,[45] which was calculated under the condition of 10 ppm cooper at room temperature (Figure S8b). Calculated after reaching an equilibrium, TpODH possessed a high K_d value of approximately 5.97×10^5 mL g^{-1}, indicating a strong affinity for copper.

As shown in Figure S8c, TpODH was determined to have a capacity of other three metallic ions, including Pb(II), Cd(II), and Cr(II), to be about 38.52, 1.34, and 0.98 mg g^{-1}, respectively. In detail, for Cr(II) and Cd(II), the adsorption capacities were not changed along with an increase of initial concentrations, indicating TpODH has a poor adsorption capacity among these.

The adsorption selectivity is very important for estimating the property of adsorbent. The selectivity test was also performed on TpODH in a mixture solution (pH = 4) containing five metal ions at the same concentration of 10 ppm. As shown in Figure 7d, TpODH exhibited more than 99% removal efficiency for Cu(II) and Hg(II) but less than 10% for other three ions Pb(II), Cr(II), and Cd(II). As a result, TpODH has a better removal ability of toxic metallic ions, including Cu(II) and Hg(II). It should be highlighted that the adsorption ability to Cu(II) was the highest in the mixture solution. The different adsorption capacity for the five different metal ions in a multicomponent system might be attributed to different inherent properties of ions, such as ionic radius, hardness, and electronegativity.[46] The pristine material with porosity and large surface area has a good removal ability to metallic ions. In detail, the nature of functional groups on the sorbent plays a vital role in selectivity adsorption, as well as the difference from their charge and radius of the hydrated ions. Based on the hard and soft acids and bases (HSAB) theory, copper is a soft metal with an especially high affinity capacity for nitrogenous ligands. Therefore, cooper presents excellent affinity in all experiments.

DOI: 10.1021/acsami.8b18502
ACS Appl. Mater. Interfaces 2019, 11, 11706−11714

Considering the robustness and stability under the harsh experimental conditions, PXRD and surface area measurements of the material were carried out after the adsorption. The results are shown in Figure S9. The diffraction patterns of PXRD show that the samples retained their crystalline structure, confirming the chemical stability of TpODH. A slight decrease of the surface area (510 $m^2 g^{-1}$ of TpODH_Cu and 361 $m^2 g^{-1}$ of TpODH_Hg) also confirmed their structure without a significant network distortion. In addition, the recycling ability of this material was inspected and the Cu-captured TpODH was regenerated by immersing in 6 mM HCl and 6 mM HNO_3, respectively. Both of the regenerated materials were then used for metal removal, and only 51 and 67% of the original capacities were retained. Thus, the recycling ability of this material is not excellent, which may be due to the narrow pore size of this kind of material.

Adsorption Mechanism. The adsorption mechanism of heavy metal ions using TpODH adsorbent relied on synergistic combination of electrostatic (between metal ion and functional groups such as amide, amino, and carbonyl groups) and coordination interactions. On the basis of the HSAB theory, the adsorption may be dominated by the coordination interaction between adsorbate and adsorbent. High-resolution FT-IR and XPS analyses of the TpODH_Cu complex were performed to confirm that. It could be seen from the FT-IR spectrum (Figure 8a), compared to Figure 2a, that the band at 3373 cm^{-1} weakened and shifted to 3320 cm^{-1} and the bands at 1540 and 1237 cm^{-1} became broader and shifted to 1519 and 1227 cm^{-1}, respectively. The shift of these bonds might reflect the electrostatic and ion-exchange interactions between metallic ions and the functional group (−NH) on the material after the replacement of hydrogen ions.[47] Meanwhile, the intensity reduction of the characteristic FT-IR signals following the adsorption of Cu(II) clearly demonstrated that the coordination interactions between Cu(II) and amide, amino, and carbonyl groups actually occurred.[48]

XPS analysis was very important for further investigation of the mechanism between Cu(II) ions and TpODH. The high-resolution XPS survey wide scan spectrum of TpODH and TpODH_Cu was obtained. As displayed in Figure S10a, there were three characteristics peaks for TpODH, C1s (284 eV), N 1s (399 eV), and O 1s (532 eV), whereas Cu 2p (933 eV) and Cl 2p (199 eV) peaks for TpODH_Cu are clearly observed in Figure S10b, besides three above-mentioned peaks, indicating that the copper ions were adsorbed on TpODH via coordination interaction.[49] Furthermore, elemental content and composition of the TpODH and TpODH_Cu samples based upon the analysis of the survey spectra are shown in Figure 8b and Table S1. High-resolution XPS spectra of TpODH and TpODH_Cu were also given. There were no characteristic peaks about copper ions in Figure 8c, whereas in Figure 8d, the binding energies in 932.5 and 952.2 correspond to the satellite peaks of Cu $2p_{3/2}$ and Cu $2p_{1/2}$, regarded as the Cu 2p peak, indicating the presence of Cu(II).[50] The satellite peaks were related to the interactions between Cu(II) and functional groups (−NH, −C═O).[51] In detail, the Cu LMM spectrum of the characteristic TpODH_Cu XPS band of Cu(II) was clearly seen in the inset of Figure 8d. A more detailed chemical analysis on XPS was obtained from the C1s spectra illustrated in Figure S11 (SI). Compared with Figure S11a,b, there were slight shifts of three characteristic peaks, manifesting that the electron cloud density of different C atoms was changed along with the adsorption process. The peak's intensity between TpODH and TpODH_Cu was further compared and is shown in Figure S11c, and was slightly decreased in the latter. As shown in Figure S12 (SI), N 1s and O 1s XPS spectra of TpODH and TpODH_Cu further confirmed that metallic ions could be adsorbed on TpODH via electrostatic interaction and coordination interaction. In addition, after the saturation adsorption of Cu(II) with TpODH, the pH of the Cu(II) solution was measured. We found that the acidity was decreased from the initial pH = 4.5 to the final pH = 1.5, further indicating hydrazone nitrogen chelation with metal along with deprotonation.[52]

CONCLUSIONS

In summary, we developed a straightforward strategy for constructing a hydrazone-linked COF using alkyl amine as a building block, which was used to adsorb metal ions. Our findings overcame the lack of building block of COF synthesis by introducing a flexible alkyl amine (ODH). The key design for alkyl amine-based COF was the introduction of Tp with the hydroxyl (−OH) moieties as the monomer, and forming an intramolecular hydrogen bonding (N−H···O═C) in the network was beneficial to improving the internal property of COF, including crystallinity, porosity, and chemical stability. The high density of N and O elements aligned in the periodic arrays on the walls of TpODH are proximate with each other, facilitating their cooperation interaction and high affinities toward the metal ions such as copper and mercury. The pseudo-second-order kinetic model was well suitable for the adsorption process, which convincingly demonstrated the coordination interaction between metallic ions (Cu(II)) and TpODH. Furthermore, this adsorption mechanism was also revealed by the FT-IR and XPS analyses. However, TFBODH had lower efficiency to remove metal ions due to lack of formation of intramolecular hydrogen bonding in the network. Therefore, it was expected that such a simple way would be explored for the construction of other COFs using alkyl amines and applied for efficient removal of heavy metal ions.

ASSOCIATED CONTENT

Supporting Information

The Supporting Information is available free of charge on the ACS Publications website at DOI: 10.1021/acsami.8b18502.

Materials, full synthesis procedures, characterizations and application, ^1H NMR and ^{13}C NMR spectra of Tp (Figure S1), PXRD patterns of TpODH (Figure S2), high-resolution FT-IR spectra of COF and monomers (Figure S3), the unit cells, molecular size, and calculated gas-phase rotational barrier (Figure S4), N_2 adsorption−desorption isotherms, pore size distribution, and specific surface area plots of COFs (Figure S5), PXRD patterns of COF after different treatments (Figure S6), TGA analysis of COFs (Figure S7), adsorption experiment data (Figure S8), PXRD pattern and N_2 adsorption−desorption isotherms (Figure S9), low-resolution XPS survey wide scans spectra (Figure S10), high-resolution XPS C1s spectra (Figure S11), high-resolution XPS N 1s and O 1s spectra (Figure S12), elemental composition (Table S1) (PDF)

DOI: 10.1021/acsami.8b18502
ACS Appl. Mater. Interfaces 2019, 11, 11706−11714

AUTHOR INFORMATION

Corresponding Authors

*E-mail: junjieou@dicp.ac.cn. Tel.: +86-411-84379576. Fax: +86-411-84379620 (J.O.).

*E-mail: ymwei@nwu.edu.cn. Tel/Fax: +86-29-81535026 (Y.W.).

ORCID

Junjie Ou: 0000-0002-1672-6119

Mingliang Ye: 0000-0002-5872-9326

Notes

The authors declare no competing financial interest.

ACKNOWLEDGMENTS

Financial support is gratefully acknowledged from the China State Key Basic Research Program Grant (2016YFA0501402) and the National Science Fund for Distinguished Young Scholars (21525524) to M.Y., as well as the National Natural Sciences Foundation of China (No. 21575141) and CAS-Weigao Research & Development Program ([2017]-009) to J.O.

REFERENCES

(1) Ascherl, L.; Sick, T.; Margraf, J. T.; Lapidus, S. H.; Calik, M.; Hettstedt, C.; Karaghiosoff, K.; Döblinger, M.; Clark, T.; Chapman, K. W.; Auras, F.; Bein, T. Molecular Docking Sites Designed for the Generation of Highly Crystalline Covalent Organic Frameworks. *Nat. Chem.* **2016**, *8*, 310−316.

(2) Côté, A. P.; B, A. I.; Ockwig, N. W.; O'Keeffe, M.; Matzger, A. J.; Yaghi, O. M. Porous, Crystalline, Covalent Organic Frameworks. *Science* **2005**, *310*, 1166−1170.

(3) Crowe, J. W.; Baldwin, L. A.; McGrier, P. L. Luminescent Covalent Organic Frameworks Containing a Homogeneous and Heterogeneous Distribution of Dehydrobenzoannulene Vertex Units. *J. Am. Chem. Soc.* **2016**, *138*, 10120−10123.

(4) Wan, S.; Guo, J.; Kim, J.; Ihee, H.; Jiang, D. A Photoconductive Covalent Organic Framework: Self-condensed Arene Cubes Composed of Eclipsed 2D Polypyrene Sheets for Photocurrent Generation. *Angew. Chem., Int. Ed.* **2009**, *48*, 5439−5442.

(5) Guo, J.; Xu, Y.; Jin, S.; Chen, L.; Kaji, T.; Honsho, Y.; Addicoat, M. A.; Kim, J.; Saeki, A.; Ihee, H.; Seki, S.; Irle, S.; Hiramoto, M.; Gao, J.; Jiang, D. Conjugated Organic Framework with Three-Dimensionally Ordered Stable Structure and Delocalized π Clouds. *Nat. Commun.* **2013**, *4*, No. 2736.

(6) Furukawa, H.; Yaghi, O. M. Storage of Hydrogen, Methane, and Carbon Dioxide in Highly Porous Covalent Organic Frameworks for Clean Energy Applications. *J. Am. Chem. Soc.* **2009**, *131*, 8875−8883.

(7) Ding, S. Y.; Gao, J.; Wang, Q.; Zhang, Y.; Song, W. G.; Su, C. Y.; Wang, W. Construction of Covalent Organic Framework for Catalysis: Pd/COF-LZU1 in Suzuki-Miyaura Coupling Reaction. *J. Am. Chem. Soc.* **2011**, *133*, 19816−19822.

(8) Colson, J. W.; Woll, A. R.; Mukherjee, A.; Levendorf, M. P.; Spitler, E. L.; S, V. B.; Spencer, M. G.; Park, J.; Dichtel, R. W. Oriented 2D Covalent Organic Framework Thin Films on Single-Layer Graphene. *Science* **2011**, *332*, 228−231.

(9) Xu, H.; Tao, S.; Jiang, D. Proton Conduction in Crystalline and Porous Covalent Organic Frameworks. *Nat. Mater.* **2016**, *15*, 722−726.

(10) Bobbitt, N. S.; Mendonca, M. L.; Howarth, A. J.; Islamoglu, T.; Hupp, J. T.; Farha, O. K.; Snurr, R. Q. Metal−Organic Frameworks for the Removal of Toxic Industrial Chemicals and Chemical Warfare Agents. *Chem. Soc. Rev.* **2017**, *46*, 3357−3385.

(11) Zhang, Y.; Wei, S.; He, Y.; Nawaz, F.; Liu, S.; Zhang, H.; Xiao, F. S. Solvothermal Synthesis of Carboxyl and Amido Functionalized Mesoporous Resins for Water Treatments. *J. Mater. Chem.* **2010**, *20*, 4609−4614.

(12) Huang, M. R.; Lu, H. J.; Li, X. G. Synthesis and Strong Heavy-Metal Ion Sorption of Copolymer Microparticles from Phenylenediamine and Its Sulfonate. *J. Mater. Chem.* **2012**, *22*, 17685−17699.

(13) Zhuang, X.; Zhao, Q.; Wan, Y. Multi-Constituent Co-Assembling Ordered Mesoporous Thiol-Functionalized Hybrid Materials: Synthesis and Adsorption Properties. *J. Mater. Chem.* **2010**, *20*, 4715−4724.

(14) Ravikumar, L.; Kalaivani, S. S.; Murugesan, A.; Vidhyadevi, T.; Karthik, G.; Kirupha, S. D.; Sivanesan, S. Synthesis, Characterization, and Heavy Metal Ion Aadsorption Studies of Polyamides, Polythioamides having Pendent Chlorobenzylidine Rings. *J. Appl. Polym. Sci.* **2011**, *122*, 1634−1642.

(15) McManamon, C.; Burke, A. M.; Holmes, J. D.; Morris, M. A. Amine-Functionalised SBA-15 of Tailored Pore Size for Heavy Metal Adsorption. *J. Colloid Interface Sci.* **2012**, *369*, 330−337.

(16) Guo, X.; Wang, C. F.; Fang, Y.; Chen, L.; Chen, S. Fast Synthesis of Versatile Nnanocrystal-Embedded Hydrogels toward the Sensing of Heavy Metal Ions and Organoamines. *J. Mater. Chem.* **2011**, *21*, 1124−1129.

(17) Nagai, A.; Guo, Z.; Feng, X.; Jin, S.; Chen, X.; Ding, X.; Jiang, D. Pore Surface Engineering in Covalent Organic Frameworks. *Nat. Commun.* **2011**, *2*, No. 1542.

(18) Bunck, D. N.; Dichtel, W. R. Postsynthetic Functionalization of 3D Covalent Organic Frameworks. *Chem. Commun.* **2013**, *49*, 2457−2459.

(19) Uribe-Romo, F. J.; Doonan, C. J.; Furukawa, H.; Oisaki, K.; Yaghi, O. M. Crystalline Covalent Organic Frameworks with Hydrazone Linkages. *J. Am. Chem. Soc.* **2011**, *133*, 11478−11481.

(20) Li, Z.; Zhi, Y.; Feng, X.; Ding, X.; Zou, Y.; Liu, X.; Mu, Y. An Azine-Linked Covalent Organic Framework: Synthesis, Characterization and Efficient Gas Storage. *Chem. - Eur. J.* **2015**, *21*, 12079−12084.

(21) Yang, D. H.; Yao, Z.-Q.; Wu, D.; Zhang, Y. H.; Zhou, Z.; Bu, X. H. Structure-Modulated Crystalline Covalent Organic Frameworks as High-Rate Cathodes for Li-ion Batteries. *J. Mater. Chem. A* **2016**, *4*, 18621−18627.

(22) Mitra, S.; Sasmal, H. S.; Kundu, T.; Kandambeth, S.; Illath, K.; Diaz Diaz, D.; Banerjee, R. Targeted Drug Delivery in Covalent Organic Nanosheets (CONs) via Sequential Postsynthetic Modification. *J. Am. Chem. Soc.* **2017**, *139*, 4513−4520.

(23) Stegbauer, L.; Hahn, M. W.; Jentys, A.; Savasci, G.; Ochsenfeld, C.; Lercher, J. A.; Lotsch, B. V. Tunable Water and CO_2 Sorption Properties in Isostructural Azine-Based Covalent Organic Frameworks through Polarity Engineering. *Chem. Mater.* **2015**, *27*, 7874−7881.

(24) Chen, G. J.; Li, X. B.; Zhao, C. C.; Ma, H. C.; Kan, J. L.; Xin, Y. B.; Chen, C. X.; Dong, Y. B. Ru Nanoparticles-Loaded Covalent Organic Framework for Solvent-Free One-Pot Tandem Reactions in Air. *Inorg. Chem.* **2018**, *57*, 2678−2685.

(25) Stegbauer, L.; Schwinghammer, K.; Lotsch, B. V. A Hydrazone-Based Covalent Organic Framework for Photocatalytic Hydrogen Production. *Chem. Sci.* **2014**, *5*, 2789−2793.

(26) Bunck, D. N.; Dichtel, W. R. Bulk Synthesis of Exfoliated Two-Dimensional Polymers Using Hydrazone-Linked Covalent Organic Frameworks. *J. Am. Chem. Soc.* **2013**, *135*, 14952−14955.

(27) Liu, W.; Su, Q.; Ju, P.; Guo, B.; Zhou, H.; Li, G.; Wu, Q. A Hydrazone-Based Covalent Organic Framework as an Efficient and Reusable Photocatalyst for the Cross-Dehydrogenative Coupling Reaction of N-Aryltetrahydroisoquinolines. *ChemSusChem* **2017**, *10*, 664−669.

(28) Das, G.; Biswal, B. P.; Kandambeth, S.; Venkatesh, V.; Kaur, G.; Addicoat, M.; Heine, T.; Verma, S.; Banerjee, R. Chemical Sensing in Two Dimensional Porous Covalent Organic Nanosheets. *Chem. Sci.* **2015**, *6*, 3931−3939.

(29) Mattia, J.; Painter, P. A Comparison of Hydrogen Bonding and Order in a Polyurethane and Poly(urethane-urea) and Their Blends with Poly(ethylene glycol). *Macromolecules* **2007**, *40*, 1546−1554.

(30) Singh, D. P.; Allam, B. K.; Singh, K. N.; Singh, V. P. Binuclear Cu(I) Complex of (N′1E,N′2E)-N′1,N′2-bis(phenyl(pyridin-2-yl)-methylene) Oxalohydrazide: Synthesis, Crystal Structure and

DOI: 10.1021/acsami.8b18502
ACS Appl. Mater. Interfaces 2019, 11, 11706−11714

Catalytic Activity for the Synthesis of 1,2,3-triazoles. *J. Mol. Catal. A: Chem.* **2015**, *398*, 158−163.
(31) Melha, K. A. Antimicrobial, Spectral, Magnetic and Thermal Studies of Cu(II), Ni(II), Co(II), UO(2)(VI) and Fe(III) Complexes of the Schiff Base Derived from Oxalylhydrazide. *J. Enzyme Inhib. Med. Chem.* **2008**, *23*, 285−295.
(32) Chen, H.; Tu, H.; Hu, C.; Liu, Y.; Dong, D.; Sun, Y.; Dai, Y.; Wang, S.; Qian, H.; Lin, Z.; Chen, L. Cationic Covalent Organic Framework Nanosheets for Fast Li-Ion Conduction. *J. Am. Chem. Soc.* **2018**, *140*, 896−899.
(33) Kandambeth, S.; Mallick, A.; Lukose, B.; Mane, M. V.; Heine, T.; Banerjee, R. Construction of Crystalline 2D Covalent Organic Frameworks with Remarkable Chemical (acid/base) Stability Via a Combined Reversible and Irreversible Route. *J. Am. Chem. Soc.* **2012**, *134*, 19524−19527.
(34) Frisch, M. J.; Trucks, G. W.; Schlegel, H. B.; Scuseria, G. E.; Ortiz, M. A. J. V.; Cioslowski, J.; Fox, D. J. *Gaussian 09*, revision D.01; Gaussian, Inc.: Wallingford, CT, 2009.
(35) DeBlase, C. R.; Silberstein, K. E.; Truong, T. T.; Abruna, H. D.; Dichtel, W. R. Beta-Ketoenamine-Linked Covalent Organic Frameworks Capable of Pseudocapacitive Energy Storage. *J. Am. Chem. Soc.* **2013**, *135*, 16821−16824.
(36) Lu, T.; Chen, F. W. Multiwfn: A Multifunctional Wavefunction Analyzer. *J. Comput. Chem.* **2012**, *33*, 580−592.
(37) Capacci-Daniel, C.; Dehghan, S.; Wurster, V. M.; Basile, J. A.; Hiremath, R.; Sarjeant, A. A.; Swift, J. A. Halogen/methyl Exchange in a Series of Isostructural 1,3-bis(m-dihalophenyl)ureas. *CrystEngComm* **2008**, *10*, 1875−1880.
(38) Zhao, C.; Diercks, C. S.; Zhu, C.; Hanikel, N.; Pei, X.; Yaghi, O. M. Urea-Linked Covalent Organic Frameworks. *J. Am. Chem. Soc.* **2018**, *140*, 16438−16441.
(39) Chandra, S.; Kundu, T.; Dey, K.; Addicoat, M.; Heine, T.; Banerjee, R. Interplaying Intrinsic and Extrinsic Proton Conductivities in Covalent Organic Frameworks. *Chem. Mater.* **2016**, *28*, 1489−1494.
(40) Sun, Q.; Aguila, B.; Perman, J.; Earl, L. D.; Abney, C. W.; Cheng, Y.; Wei, H.; Nguyen, N.; Wojtas, L.; Ma, S. Postsynthetically Modified Covalent Organic Frameworks for Efficient and Effective Mercury Removal. *J. Am. Chem. Soc.* **2017**, *139*, 2786−2793.
(41) Huang, N.; Zhai, L.; Xu, H.; Jiang, D. Stable Covalent Organic Frameworks for Exceptional Mercury Removal from Aqueous Solutions. *J. Am. Chem. Soc.* **2017**, *139*, 2428−2434.
(42) Yan, M. K.; Zheng, C.; Yin, J.; An, Z. F.; Chen, R. F.; Feng, X. M.; Song, J.; Fan, Q. L.; Huang, W. Theoretical Study of Organic Molecules Containing N or S Atoms as Receptors for Hg(II) Fluorescent Sensors. *Synth. Methods* **2012**, *162*, 641−649.
(43) Niu, L.; Deng, S.; Yu, G.; Huang, J. Efficient Removal of Cu(II), Pb(II), Cr(VI) and As(V) from Aqueous Solution Using an Aminated Resin Prepared by Surface-Initiated Atom Transfer Radical Polymerization. *Chem. Eng. J.* **2010**, *165*, 751−757.
(44) Li, Y. H.; Ding, J.; Luan, Z.; Di, Z.; Zhu, Y.; Xu, C.; Wu, D.; Wei, B. Competitive Adsorption of Pb^{2+}, Cu^{2+} and Cd^{2+} Ions from Aqueous Solutions by Multiwalled Carbon Nanotubes. *Carbon* **2003**, *41*, 2787−2792.
(45) Yantasee, W.; Warner, C. L.; Sangvanich, T.; Addleman, R. S.; Carter, T. G.; Wiacek, R. J.; Fryxell, G. E.; Timchalk, C.; Warner, M. G. Removal of Heavy Metals from Aqueous Systems with Thiol Functionalized Superparamagnetic Nanoparticles. *Environ. Sci. Technol.* **2007**, *41*, 5114−5119.
(46) Zhu, Q.; Li, Z. K. Hydrogel-Supported Nanosized Hydrous Manganese Dioxide: Synthesis, Characterization, and Adsorption Behavior Study for Pb^{2+}, Cu^{2+}, Cd^{2+} and Ni^{2+} Removal from Water. *Chem. Eng. J.* **2015**, *281*, 69−80.
(47) Tan, P.; Wen, J.; Hu, Y.; Tan, X. Adsorption of $Cu^{2+}$and Cd^{2+} From Aqueous Solution by Novel Electrospun Poly(vinyl alcohol)/Graphene Oxide Nanofibers. *RSC Adv.* **2016**, *6*, 79641−79650.
(48) Chen, Y.; He, M.; Wang, C.; Wei, Y. A Novel Polyvinyltetrazole-Grafted Resin with High Capacity for Adsorption of Pb(ii), Cu(ii) and Cr(iii) Ions from Aqueous Solutions. *J. Mater. Chem. A* **2014**, *2*, 10444−10453.
(49) Zhang, S.; Niu, Q.; Lan, L.; Li, T. Novel Oligothiophene-Phenylamine Based Schiff Base as a Fluorescent Chemosensor for the Dual-Channel Detection of Hg^{2+} and Cu^{2+} with High Sensitivity and Selectivity. *Sens. Actuators, B* **2017**, *240*, 793−800.
(50) Mai, H.; Zhang, D.; Shi, L.; Yan, T.; Li, H. Highly Active $Ce_{1-x}Cu_xO_2$ Nanocomposite Catalysts for the Low Temperature Oxidation of CO. *Appl. Surf. Sci.* **2011**, *257*, 7551−7559.
(51) Li, J.; Chen, S.; Sheng, G.; Hu, J.; Tan, X.; Wang, X. Effect of Surfactants on Pb(II) Adsorption from Aqueous Solutions Using Oxidized Multiwall Carbon Nanotubes. *Chem. Eng. J.* **2011**, *166*, 551−558.
(52) Merí-Bofí, L.; Royuela, S.; Zamora, F.; Ruiz-González, M. L.; Segura, J. L.; Muñoz-Olivas, R.; Mancheño, M. J. Thiol Grafted Imine-Based Covalent Organic Frameworks for Water Remediation Through Selective Removal of Hg(ii). *J. Mater. Chem. A* **2017**, *5*, 17973−17981.

DOI: 10.1021/acsami.8b18502
ACS Appl. Mater. Interfaces 2019, 11, 11706−11714